Precision gluino mass at the CERN LHC in supersymmetric models with decoupled scalars

Howard Baer,[1,2,*] Vernon Barger,[2,†] Gabe Shaughnessy,[2,‡] Heaya Summy,[1,§] and Lian-Tao Wang[3,‖]

[1]*Dept. of Physics, Florida State University, Tallahassee, Florida 32306, USA*
[2]*Dept. of Physics, University of Wisconsin, Madison, Wisconsin 53706, USA*
[3]*Department of Physics, Princeton University, Princeton, New Jersey 08543, USA*

(Received 5 April 2007; published 29 May 2007)

One way to ameliorate the SUSY flavor and *CP* problems is to postulate that scalar masses lie in the TeV or beyond regime. For example, the focus point (FP) region of the minimal supergravity (mSUGRA) model is especially compelling in that heavy scalar masses can coexist with low fine-tuning while yielding the required relic abundance of cold dark matter (via a mixed Higgsino-bino neutralino). We examine many of the characteristics of collider events expected to arise at the CERN LHC in models with multi-TeV scalars, taking the mSUGRA FP region as a case study. The collider events are characterized by a hard component arising from gluino pair production, plus a soft component arising from direct chargino and neutralino production. Gluino decays in the FP region are characterized by lengthy cascades yielding very large jet and lepton multiplicities, and a large b-jet multiplicity. Thus, as one steps to higher jet, b-jet or lepton multiplicity, signal-over-background rates should steadily improve. The lengthy cascade decays make mass reconstruction via kinematic edges difficult; however, since the hard component is nearly pure gluino pair production, the gluino mass can be extracted to $\pm 8\%$ via total rate for $E_T^{\rm miss}+ \geq 7$-jet$+ \geq 2b$-jet events, assuming 100 fb^{-1} of integrated luminosity. The distribution of invariant mass of opposite-sign/same-flavor dileptons in the hard component exhibits two dilepton mass edges: $m_{\tilde{Z}_2} - m_{\tilde{Z}_1}$ and $m_{\tilde{Z}_3} - m_{\tilde{Z}_1}$. As a consistency check, the same mass edges should be seen in isolated opposite-sign dileptons occurring in the soft component trilepton signal which originates mainly from chargino-neutralino production.

DOI: 10.1103/PhysRevD.75.095010 PACS numbers: 14.80.Ly, 11.30.Pb, 12.60.Jv, 13.85.Rm

I. INTRODUCTION

The minimal supergravity (mSUGRA) model [1–3] is a well-motivated supersymmetric model with a small parameter space that forms a template for many investigations of the phenomenological consequences of weak scale supersymmetry. In mSUGRA, it is assumed that the minimal supersymmetric standard model, or MSSM, is a valid effective theory of physics between the energy scales $Q = M_{\rm GUT}$ and $Q = M_{\rm weak}$. It is further assumed that all MSSM scalar masses unify to a common value m_0 at $M_{\rm GUT}$, while gauginos unify to a common value $m_{1/2}$ and trilinear soft terms unify to a common value A_0. The weak scale soft parameters can be calculated by renormalization group evolution from $M_{\rm GUT}$ to $M_{\rm weak}$. The large value of the top quark Yukawa coupling drives the up-Higgs squared mass to negative values, leading to radiative electroweak symmetry breaking (EWSB). The EWSB minimization conditions allow one to trade the bilinear soft breaking term B for $\tan\beta$, the ratio of Higgs field vevs. It also determines the magnitude (but not the sign) of the superpotential Higgs mass term μ. Thus, the entire weak scale sparticle mass spectrum and mixings can be calculated from the well-known parameter set

$$m_0, \quad m_{1/2}, \quad A_0, \quad \tan\beta, \quad \mathrm{sign}(\mu). \tag{1}$$

Thus, once this parameter set is stipulated, a whole host of observables, including the neutralino dark matter relic density $\Omega_{\tilde{Z}_1}h^2$ and collider scattering events, may be calculated. For implementation, we use Isajet v7.74 [4,5] to calculate the sparticle mass spectrum and associated collider events, and IsaReD [6] to calculate the neutralino relic density.

One of the important consequences of the MSSM, due to R-parity conservation, is that the lightest SUSY particle (LSP) is absolutely stable. In mSUGRA, the LSP is usually found to be the lightest neutralino $\tilde{Z}_1$, which is a weakly interacting massive particle (WIMP), and hence has the potential to naturally match the measured abundance of cold dark matter in the universe. An analysis of the three-year WMAP and galaxy survey data sets [7] implies that the ratio of dark matter density to critical density,

$$\Omega_{\tilde{Z}_1}h^2 \equiv \rho_{\tilde{Z}_1}/\rho_c = 0.111^{+0.011}_{-0.015} \qquad (2\sigma). \tag{2}$$

where $h = 0.74 \pm 0.03$ is the Hubble constant. By comparing the mSUGRA predicted value of $\Omega_{\tilde{Z}_1}h^2$ to this measured value, one finds that only certain parts of the mSUGRA parameter space are cosmologically allowed. These include the following.

(i) The bulk region at low m_0 and low $m_{1/2}$, where neutralino annihilation is enhanced by light t-channel slepton exchange [8]. The tight WMAP $\Omega_{\rm CDM}h^2$ limit has pushed this allowed region to very

*Electronic address: baer@hep.fsu.edu
†Electronic address: barger@physics.wisc.edu
‡Electronic address: gshau@hep.wisc.edu
§Electronic address: heaya.summy@gmail.com
‖Electronic address: lianwang@princeton.edu

small m_0 and $m_{1/2}$ values, while LEP2 limits on $m_{\tilde{W}_1}$ and $m_{\tilde{\ell}}$ (and possibly on m_h) have excluded these same low values so that almost no bulk region has survived [9].

(ii) The stau coannihilation region occurs at very low m_0 but any $m_{1/2}$ values, so that $m_{\tilde{\tau}_1} \simeq m_{\tilde{Z}_1}$, and neutralinos can annihilate against tau sleptons [10] in the early universe. For certain A_0 values which dial $m_{\tilde{t}_1}$ to very low values, there also exists a top-squark coannihilation region [11].

(iii) The A-funnel region occurs at large values of the parameter $\tan\beta \sim 50$, where $2m_{\tilde{Z}_1} \sim m_A$, and neutralinos can annihilate through the broad pseudoscalar Higgs resonance [12]. There is also a light Higgs resonance region where $2m_{\tilde{Z}_1} \sim m_h$ at low $m_{1/2}$ values [8,13].

(iv) At large m_0 near the boundary of parameter space, the superpotential Higgsino mass term μ becomes quite small, and the $\tilde{Z}_1$ can become a mixed Higgsino-bino neutralino. This region is known as the hyperbolic branch/focus point region (HB/FP) [14–16]. In this case, neutralino annihilation to vector bosons is enhanced, and a match to the WMAP measured relic density can be found.

The HB/FP region of mSUGRA is especially compelling. In this region, the large value of $m_0 \sim$ several TeV means that possible SUSY contributions to various flavor-changing and CP-violating processes are suppressed by the large squark and slepton masses. For instance, SUSY contributions to the flavor-violating decay $b \to s\gamma$ are small, so in the HB/FP region this decay rate is predicted to be in accord with SM predictions, as observed. Meanwhile, the calculated amount of fine-tuning in the electroweak sector has been shown to be small [14,15], in spite of the presence of multi-TeV top squarks.

In this paper, we examine the HB/FP region with regard to what sort of collider events are expected at the CERN LHC pp collider, which is set to begin operating in the near future at a center-of-mass energy $\sqrt{s} = 14$ TeV. Much previous work on this issue has been done. In Refs. [17,18], the reach of the LHC in the mSUGRA model, including the HB/FP region, was calculated. The reach for 100 fb^{-1} was found to extend to $m_{1/2} \sim$ 700 GeV, corresponding to a reach in $m_{\tilde{g}}$ of about 1.8 TeV. The reaches of $\sqrt{s} = 0.5$ and 1 TeV e^+e^- linear colliders were also calculated [19], and found to extend past that of the LHC, since when μ becomes small, charginos become light, and chargino pair production is a reaction that e^+e^- colliders are sensitive to, essentially up to the kinematic limit for chargino pair production. In fact, the reach of the Fermilab Tevatron for SUSY in the clean trilepton channel [20,21] is somewhat enhanced in the HB/FP region [22], since charginos and neutralinos can be quite light, and decay with characteristic dilepton mass edges. The reaches of direct [23] and indirect [24] dark matter search experiments are also enhanced in the HB/FP region.

In Ref. [25], Hinchliffe and Paige examined characteristic measurements that the LHC could make for an mSUGRA sample point nearby to the HB/FP region. They found a good signal/background ratio could be obtained with a hard cut on effective mass $M_{\rm eff} = \sum_{\rm jets} E_T + \sum_{\rm leptons} E_T + E_T^{\rm miss}$ (e.g. $M_{\rm eff} > 400$ GeV) and by requiring the presence of a b-jet.[1] Some characteristic distributions such as $m(\ell^+\ell^-)$ which gave a dilepton mass edge at $m_{\tilde{Z}_2} - m_{\tilde{Z}_1}$ and $m(b-{\rm jet},\ell) < \sqrt{(m_t^2 - M_W^2)/2}$ (indicating the presence of a t-quark in the decay chain) could be made. In Ref. [27], methods for extracting $m_{\tilde{g}}$ were examined for the stau coannihilation region.

In Ref. [28], it was noted that collider signatures in the HB/FP region gave rise to large b-jet multiplicities, which could be exploited to enhance signal over background. In Ref. [29], Mizukoshi, Mercadante and Tata found that the LHC reach in the HB/FP region could be enhanced by up to 20% by requiring events with the presence of one or two tagged b-jets. In Ref. [30], a model-independent exploration of the HB/FP region was made with regard to collider and dark matter signals. The LHC reach via multilepton cascade decays was compared to the LHC reach via clean trileptons from $pp \to \tilde{W}_1\tilde{Z}_2 \to 3\ell + E_T^{\rm miss}$ production. In the latter process, backgrounds from W^*Z^* and $W^*\gamma^*$ were calculated, and the trilepton reach was found to be comparable to—but slightly smaller than—the reach via a search for gluino cascade decays. In Ref. [31], the authors examined what sort of cosmological measurements could be made in several mSUGRA case studies (including the point[2] LCC2 in the HB/FP region) by measurements at the LHC and a $\sqrt{s} = 0.5$ and 1 TeV ILC. For LCC2 at the LHC, they assumed the $\tilde{Z}_3 - \tilde{Z}_1$ and $\tilde{Z}_2 - \tilde{Z}_1$ mass edges could be measured to an accuracy of 1 GeV, while it was conjectured that $m_{\tilde{g}}$ and $m_{\tilde{Z}_1}$ could be measured to $\sim$10% accuracy via some kinematic distributions.

In this paper, in anticipation of the LHC turn on, we wish to understand many of the characteristics of collider events expected in the HB/FP region, with an eye towards sparticle mass measurements rather than reach studies. We find that the expected collider events in the HB/FP region separate themselves into a hard component, arising from gluino pair production, and a soft component, arising from pair production of charginos and neutralinos. The gluino pair production events typically involve lengthy cascade decays to top and bottom quarks [32], and so high jet, b-jet and isolated lepton multiplicities are expected. However, the complex cascade decays do not lend themselves to simple kinematic measurements of the gluino or neutralino

[1]The effective mass was introduced and used in heavy top quark production [26].

[2]The parameters of the point are $m_0 = 3280$ GeV, $m_{1/2} = 300$ GeV, $\tan\beta = 10$, $A_0 = 0$ GeV and $\mu > 0$.

masses, mainly due to the combinatorics of picking out the correct gluino decay products.[3] We do find that the gluino mass should be extractable based on total rate in the multijet + multilepton + $E_T^{\rm miss}$ events to a precision of about 5–10% for 100 fb^{-1} of integrated luminosity. For both the hard and soft components, the $\tilde{Z}_3 - \tilde{Z}_1$ and $\tilde{Z}_2 - \tilde{Z}_1$ mass edges should be visible.

The remainder of this paper is organized as follows. In Sec. II, we present details of sparticle masses and cross sections expected from the HB/FP region at the LHC. In Sec. III, we present some details of our signal and background calculations. In Sec. IV we present distributions for a variety of collider observables for a case study and SM backgrounds. We present a set of cuts that allows good separation of signal vs background over a large range of $m_{\tilde{g}}$ values. In Sec. V, we show expected signal-to-background plots for gluino pair production and discuss how these can be used to extract a measurement of the gluino mass. In Sec. VI, we address leptonic signals. We conclude in Sec. VII.

II. SPARTICLE PRODUCTION AND DECAY IN THE HB/FP REGION

In the mSUGRA model, for a given set of GUT scale soft SUSY breaking (SSB) masses, the associated weak scale values may be computed via renormalization group (RG) evolution [35]. Once the weak scale SSB terms have been obtained, then the scalar potential must be minimized to determine if electroweak symmetry is properly broken. While one EWSB condition allows the bilinear parameter B to be traded for $\tan\beta$, the other condition reads (at one-loop)

$$\mu^2 = \frac{m_{H_d}^2 - m_{H_u}^2 \tan^2\beta}{(\tan^2\beta - 1)} - \frac{M_Z^2}{2}, \qquad (3)$$

which determines the magnitude of the superpotential μ parameter. Thus, one condition that EWSB is successfully broken is that a positive value of μ^2 has been generated. Roughly, if all the soft parameters entering Eq. (3) are of order M_Z^2, then naturalness is satisfied, and the model is not fine-tuned.

For a fixed value of the parameter $m_{1/2}$ in the mSUGRA model, if m_0 is taken to be of order the weak scale, then $m_{H_u}^2$ is driven to negative values at the weak scale owing to the push from the large top quark Yukawa coupling in the RGEs. However, if m_0 is taken too large, then the GUT scale value of $m_{H_u}^2$ is so high that it is not driven to negative values when the weak scale is reached in RG running, and a positive value of μ^2 cannot be found. Intermediate to these two extreme cases must exist a region where μ^2 is found to be zero, which forms the large m_0 edge of parameter space. If μ^2 is positive, but tiny, then extremely light Higgsino-like charginos will be generated, in conflict with bounds from LEP2, which require $m_{\tilde{W}_1} > 103.5$ GeV. If μ^2 is large enough to evade LEP2 limits, then large Higgsino-bino mixing occurs in the chargino and neutralino sectors, and in fact the lightest neutralino becomes a mixed Higgsino-bino dark matter particle. A lightest neutralino of mixed Higgsino-bino form has a large annihilation rate to vector bosons in the early universe, and hence may have a dark matter relic density in accord with WMAP measurements. In this region, dubbed the hyperbolic branch/focus point region, multi-TeV squark and slepton masses can coexist with low fine-tuning as dictated by Eq. (3). Thus, the HB/FP region is characterized by TeV-scale squark and slepton masses, which are useful for suppressing possible FCNC or CP-violating processes, low fine-tuning, and a dark matter relic density in accord with WMAP. Given these qualities, it is important to investigate what HB/FP supersymmetry events would look like at the LHC collider and what sort of mass measurements could be made in this region.

We have generated sparticle mass spectra in the HB/FP region using Isajet v7.74, retaining only points which yield a relic density $\Omega_{\tilde{Z}_1} h^2 \sim 0.11$. These points and the anticipated measurement uncertainty are listed in Table I. Since the scalar quarks are decoupled, the gluino decays via suppressed 3-body decays, making the gluino width small and not a significant source of mass measurement uncertainty. In Fig. 1, we show the points in the HB/FP from Table I in the m_0 vs $m_{1/2}$ plane. Isajet uses two-loop RGEs for the scalar mass evolution, and minimizes the RG-improved one-loop effective potential at an optimized scale $Q = \sqrt{m_{\tilde{t}_L} m_{\tilde{t}_R}}$ (which accounts for leading two-loop effects). A unique feature of Isajet's sparticle mass algorithm is that it decouples various SSB terms from the RG evolution at their own mass scales, which gives a more gradual

TABLE I. Points in the HB/FP region that yield a relic density $\Omega_{\tilde{Z}_1} h^2 \sim 0.11$. Common values of $\tan\beta = 30$, $A_0 = 0$, $\mu > 0$ and $m_t = 175$ GeV are assumed. The gluino mass in GeV and its anticipated measurement uncertainty at the LHC are also given. The total gluino width is given in MeV.

Point	m_0	$m_{1/2}$	$M_{\tilde{g}}$	$\delta M_{\tilde{g}}/M_{\tilde{g}}$	$\Gamma_{\tilde{g}}$
FP0	2300	200	591	LEP2 excl.	0.2
FP1	2450	225	655	LEP2 excl.	0.4
FP2	2550	250	717	±10%	0.6
FP3	2700	300	838	±8%	1.1
FP4	2910	350	959	±7%	1.8
FP5	3050	400	1076	±8%	2.7
FP6	3410	500	1310	±8%	5.1
FP7	3755	600	1540	—	8.1
FP8	4100	700	1766	—	11.8
FP9	4716	900	2211	—	20.7

[3]Studies of gluino mass [33] and spin [34] determination have been made through the cascade decays $\tilde{g} \to b\bar{b}\tilde{Z}_2^*$ with $\tilde{b}_1 \to \tilde{Z}_2 \to \tilde{l} \to \tilde{Z}_1$ at parameter point SPS1a.

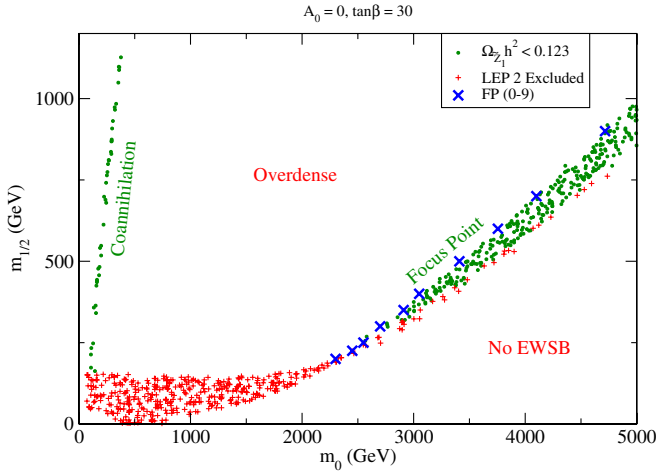

FIG. 1 (color online). Regions of allowed relic density in the m_0 vs $m_{1/2}$ plane for $A_0 = 0$, $\tan\beta = 30$ and $m_t = 175$ GeV. Points in the HB/FP region from Table I that are consistent with the observed relic density $\Omega_{\tilde{Z}_1} h^2 \sim 0.11$ are shown by a blue x. The white region above the focus point and surrounding the coannihilation region give and overdensity of neutralino dark matter.

transition from the MSSM to the SM effective theory, as opposed to other approaches which use an "all-at-once" transition. Thus, the Isajet algorithm should give a good representation of sparticle mass spectra in cases that involve a severely split mass spectrum, such as in the HB/FP region.

In Fig. 2, we show the sparticle mass spectra as a function of $m_{1/2}$ along a line with $\Omega_{\tilde{Z}_1} h^2 \sim 0.11$, for $\tan\beta = 30$, $A_0 = 0$ and $\mu > 0$. The physics in the HB/FP region is not very sensitive to $\tan\beta$ or A_0, since the scalar masses effectively decouple. We take $m_t = 175$ GeV, but note that the m_0 value needed to obtain the correct relic

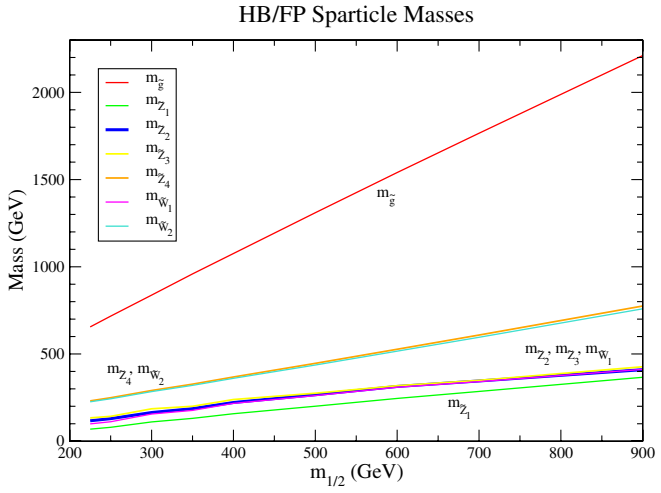

FIG. 2 (color online). Sparticle masses vs $m_{1/2}$ along lines with constant $\Omega_{\tilde{Z}_1} h^2 = 0.11$ in the HB/FP region of mSUGRA with $A_0 = 0$, $\tan\beta = 30$, $\mu > 0$ and $m_t = 175$ GeV.

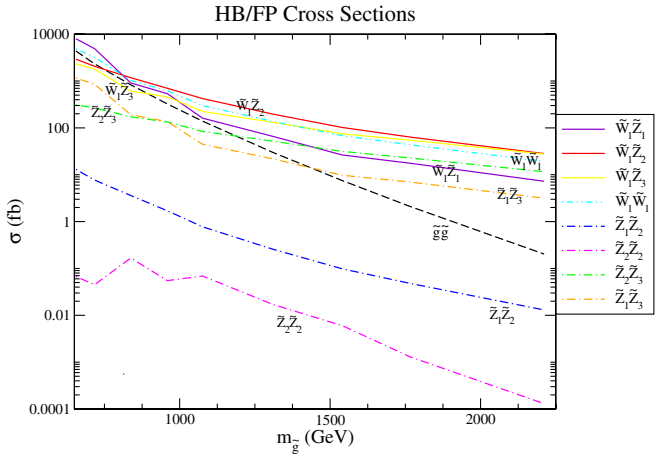

FIG. 3 (color online). Selected sparticle pair production cross sections vs $m_{\tilde{g}}$ along a line of constant $\Omega_{\tilde{Z}_1} h^2 = 0.11$ in the HB/FP region of mSUGRA with $A_0 = 0$, $\tan\beta = 30$, $\mu > 0$ and $m_t = 175$ GeV.

density is extremely sensitive to the value of m_t used, as shown in Ref. [22]. In our case, since the scalar masses are expected to decouple, the m_t dependence should not matter greatly for the phenomenology of interest.[4]

While squarks, sleptons and heavy Higgs scalars range in mass from 2.5–4.5 TeV along the range of $m_{1/2}$ shown in Fig. 2, the $\tilde{g}$ remains relatively light, of order 650–2200 GeV. In addition, since μ and $m_{1/2}$ are low, the charginos and neutralinos are *all* quite light, and possibly accessible to LHC experiments. The lower edge of the plot where $m_{1/2} \lesssim 250$ GeV is excluded by the LEP2 constraint on the chargino mass.

In Fig. 3, we show sparticle pair production rates as a function of $m_{\tilde{g}}$ in the HB/FP region. While the production cross sections are evaluated at lowest order in perturbation theory, we adopt a renormalization/factorization scale choice $Q = (m_1 + m_2)/4$ for the gluino pair production cross section which gives good agreement between LO and NLO results [37].[5] For low values of $m_{\tilde{g}} \sim 700$ GeV, gluino pair production is in the pb range, while a variety of chargino and neutralino production processes (e.g. $\tilde{W}_1\tilde{Z}_{1,2,3}$ and $\tilde{W}_1^+\tilde{W}_1^-$ production) have comparable rates. For higher values of $m_{\tilde{g}}$, the gluino pair production cross section drops quickly, and is below the fb level for $m_{\tilde{g}} > 1900$ GeV. The various chargino and neutralino production rates drop less quickly, and turn out to be by far the dominant sparticle production cross sections for $m_{\tilde{g}} \gtrsim 1.5$ TeV.

[4]In our study, we adopt the reference value $m_t = 175$ GeV to allow comparisons with other studies. The recent world average for the t-quark mass is $m_t = 171.4$ GeV [36].

[5]NLO gluino, chargino and neutralino cross sections are shown versus weak scale gaugino mass M_1 in the HB/FP region in Ref. [30].

TABLE II. Selected branching fractions of the $\tilde{g}$ for FP5 case study with parameters $m_0 = 3050$ GeV, $m_{1/2} = 400$ GeV, $A_0 = 0$, $\tan\beta = 30$ and $\mu > 0$.

mode	BF
$\tilde{g} \to t\bar{t}\tilde{Z}_1$	3.9%
$\tilde{g} \to t\bar{t}\tilde{Z}_2$	14.2%
$\tilde{g} \to t\bar{t}\tilde{Z}_3$	15.0%
$\tilde{g} \to t\bar{t}\tilde{Z}_4$	5.6%
$\tilde{g} \to t\bar{b}\tilde{W}_1 + \text{c.c}$	26.8%
$\tilde{g} \to t\bar{b}\tilde{W}_2 + \text{c.c.}$	13.9%

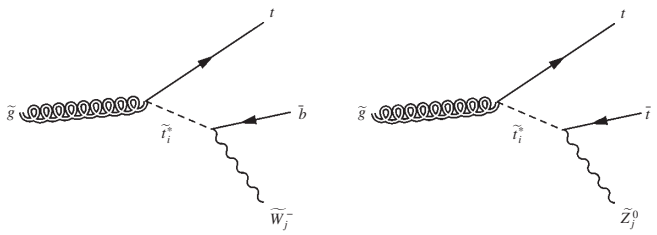

FIG. 4. Feynman diagrams of dominant gluino decays in the HB/FP region.

In the WMAP-allowed HB/FP region, since squarks have masses in the TeV range, only three-body decay modes of the gluino are allowed. Moreover, since the μ parameter is small and the lighter inos have a large Higgsino component, the third generation quark-squark-ino couplings are enhanced by top quark Yukawa coupling terms [38,39], and gluinos dominantly decay to third generation particles, especially the top quark. Thus, the dominant gluino decays modes in the HB/FP region consist of $\tilde{g} \to t\bar{t}\tilde{Z}_i$ or $t\bar{b}\tilde{W}_j$. Some major $\tilde{g}$ branching fractions are listed in Table II for a case study which we label as FP5 with $m_{\tilde{g}} = 1076$ GeV. The Feynman diagrams of these dominant decay modes are shown in Fig. 4. Thus, we expect in the HB/FP region that $pp \to \tilde{g}\,\tilde{g}\,X$ will yield events with very large jet and b-jet multiplicities, and isolated leptons. However, the combinatoric backgrounds will likely make kinematic reconstruction of mass edges which depend on $m_{\tilde{g}}$ very difficult. Meanwhile, for the same case study as in Table II, since $\tilde{Z}_2 \to e^+e^-\tilde{Z}_1$ and $\tilde{Z}_3 \to e^+e^-\tilde{Z}_1$ both occur at a branching fraction of 3.4%, it might be possible to see both the $\tilde{Z}_2 - \tilde{Z}_1$ and $\tilde{Z}_3 - \tilde{Z}_1$ mass edges in distributions of invariant opposite-sign/same-flavor isolated dileptons.

III. HB/FP SIGNAL AND BACKGROUND EVENT GENERATION

We use Isajet 7.74 [4] for the simulation of signal and background events at the LHC. A toy detector simulation is employed with calorimeter cell size $\Delta\eta \times \Delta\phi = 0.05 \times 0.05$ and $-5 < \eta < 5$. The HCAL energy resolution is taken to be $80\%/\sqrt{E} + 3\%$ for $|\eta| < 2.6$ and FCAL is $100\%/\sqrt{E} + 5\%$ for $|\eta| > 2.6$. The ECAL energy resolution is assumed to be $3\%/\sqrt{E} + 0.5\%$. We use a UA1-like jet finding algorithm with jet cone size $R = 0.4$ and require that $E_T(\text{jet}) > 50$ GeV and $|\eta(\text{jet})| < 3.0$. Leptons are considered isolated if they have $p_T(e \text{ or } \mu) > 20$ GeV and $|\eta| < 2.5$ with visible activity within a cone of $\Delta R < 0.2$ of $\Sigma E_T^{\text{cells}} < 5$ GeV. The strict isolation criterion helps reduce multilepton backgrounds from heavy quark ($c\bar{c}$ and $b\bar{b}$) production.

We identify a hadronic cluster with $E_T > 50$ GeV and $|\eta(j)| < 1.5$ as a b-jet if it contains a B hadron with $p_T(B) > 15$ GeV and $|\eta(B)| < 3$ within a cone of $\Delta R < 0.5$ about the jet axis. We adopt a b-jet tagging efficiency of 60%, and assume that light quark and gluon jets can be mistagged as b-jets with a probability $1/150$ for $E_T < 100$ GeV, $1/50$ for $E_T > 250$ GeV, with a linear interpolation for 100 GeV $< E_T <$ 250 GeV.

We have generated 200 K events each for a variety of $m_{1/2}$ values in the HB/FP region restricted to have $\Omega_{\tilde{Z}_1}h^2 \sim 0.11$. In addition, we have generated background events using Isajet for QCD jet production (jet-types include g, u, d, s, c and b quarks) over five p_T ranges as shown in Table III. Additional jets are generated via parton showering from the initial and final state hard scattering subprocesses. We have also generated backgrounds in the W + jets, Z + jets, $t\bar{t}(175)$ and WW, WZ, ZZ channels at the rates shown in Table III. The W + jets and Z + jets backgrounds use exact matrix elements for one parton emission, but rely on the parton shower for subsequent emissions.

IV. EVENT CHARACTERISTICS IN THE HB/FP REGION

We begin by applying a set of precuts to our event samples, which we list as cuts set C1 [40]: *C1 Cuts:*

$$E_T^{\text{miss}} > (100 \text{ GeV}, 0.2M_{\text{eff}}), \tag{4}$$

$$n(\text{jets}) \geq 4, \tag{5}$$

$$E_T(j1, j2, j3, j4) > 100, 50, 50, 50 \text{ GeV}, \tag{6}$$

$$S_T > 0.2. \tag{7}$$

Here, M_{eff} is defined as in Hinchliffe *et al.* [40] as $M_{\text{eff}} = E_T^{\text{miss}} + E_T(j1) + E_T(j2) + E_T(j3) + E_T(j4)$, where $j1 - j4$ refer to the four highest E_T jets ordered from highest to lowest E_T, E_T^{miss} is missing transverse energy and S_T is transverse sphericity.[6] The event rates in fb are listed after C1 in Table III, and we find that signal with these cuts is

[6]Sphericity is defined, e.g. in Ref. [41]. Here, we restrict its construction to using only transverse quantities, as is appropriate for a hadron collider.

TABLE III. Events generated and cross sections for various SM background processes plus one HB/FP case study FP5 with $m_0 = 3050$ GeV, $m_{1/2} = 400$ GeV, $A_0 = 0$, $\tan\beta = 30$ and $\mu > 0$. The C1 cuts are specified in Eqs. (4)–(7).

process	events	σ (fb)	cuts C1 (fb)
QCD (p_T: 50–100 GeV)	10^6	2.6×10^{10}	–
QCD (p_T: 100–200 GeV)	10^6	1.5×10^9	1513.3
QCD (p_T: 200–400 GeV)	10^6	7.3×10^7	3873.7
QCD (p_T: 400–1000 GeV)	10^6	2.7×10^6	486.0
QCD (p_T: 1000–2400 GeV)	10^6	1.5×10^4	4.4
W + jets; $W \to e$, μ, τ ($p_T(W)$: 100–4000 GeV)	5×10^5	3.9×10^5	1815.9
Z + jets; $Z \to \tau\bar{\tau}$, νs ($p_T(Z)$: 100–3000 GeV)	5×10^5	1.4×10^5	845.3
$t\bar{t}$	3×10^6	4.6×10^5	6415.8
WW, ZZ, WZ	5×10^5	8.0×10^4	9.3
signal (FP5: $m_{\tilde{g}} = 1076$ GeV)	2×10^5	1.2×10^3	77.5

swamped by various SM backgrounds, especially those from QCD multijet production and $t\bar{t}$ production.

Next, we investigate a variety of distributions. We show in Fig. 5 the $M_{\rm eff}$ distribution after using C1. The gray histogram denotes the sum of all backgrounds, while individual BG contributions are identified by the legend. The signal for case study FP5 is denoted by the purple histogram. In many models investigated by Hinchliffe *et al.*, it was found that signal emerges from BG at an $M_{\rm eff}$ value near the peak of the distribution, which in fact provides a rough estimate of the strongly interacting sparticle masses involved in the production subprocess. In the HB/FP region, however, squarks have decoupled from the hadronic sparticle production cross section, so only gluino pair production contributes. In addition, since in the HB/FP region gluinos decay via three-body modes, the average jet E_T is reduced significantly compared to SUSY cases with similar sparticle masses but with dominantly 2-body decays. Hence, in the HB/FP region, the $M_{\rm eff}$ distribution from the signal is typically buried beneath SM BG. In addition, for this case study, we see some structure to the $M_{\rm eff}$ distribution in the form of two separate peaks (which stand out more clearly on a linear scale, when BG is neglected). The peak near $M_{\rm eff} \sim 500$ GeV comes dominantly from the *soft* signal component, which is mainly high p_T chargino and neutralino production, which after all is the dominant sparticle production process in the HB/FP region. A second peak around $M_{\rm eff} \sim 1200$ GeV comes from gluino pair production, which we denote as the *hard* component of the signal.

We noted earlier, based on an examination of gluino decay modes in the HB/FP region, that LHC collider events ought to be characterized by large jet multiplicity, large b-jet multiplicity and large isolated lepton multiplicity. With this in mind, we show in Fig. 6 the multiplicity of jets expected from signal and from SM BG, after cuts C1.

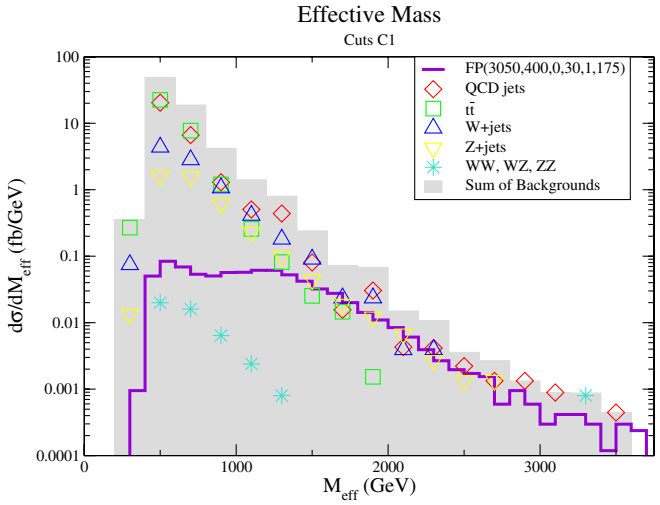

FIG. 5 (color online). Distribution of $M_{\rm eff}$ from the FP5 case study with $m_0 = 3050$ GeV, $m_{1/2} = 400$ GeV, $A_0 = 0$, $\tan\beta = 30$, $\mu > 0$ and $m_t = 175$ GeV (where $m_{\tilde{g}} = 1076$ GeV), versus various SM backgrounds.

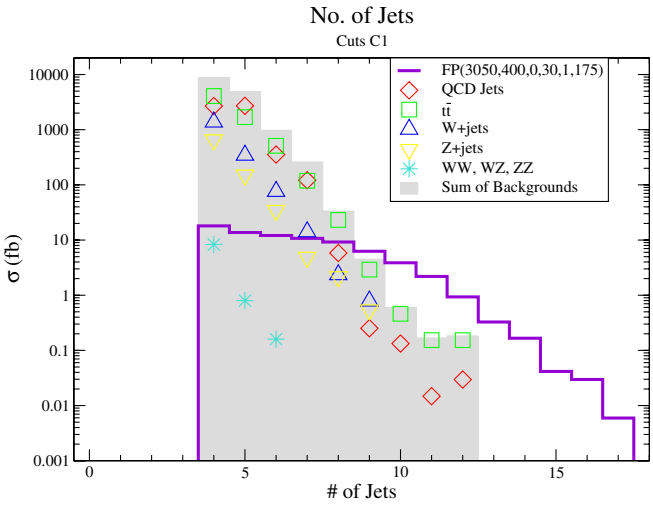

FIG. 6 (color online). Distribution of number of jets in the FP5 case study with $m_0 = 3050$ GeV, $m_{1/2} = 400$ GeV, $A_0 = 0$, $\tan\beta = 30$, $\mu > 0$ and $m_t = 175$ GeV (where $m_{\tilde{g}} = 1076$ GeV), versus various SM backgrounds.

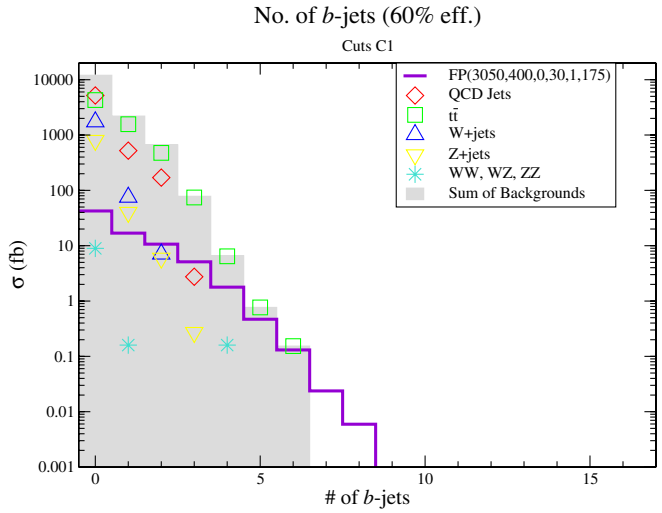

FIG. 7 (color online). Distribution of number of b-jets for the FP5 case study with $m_0 = 3050$ GeV, $m_{1/2} = 400$ GeV, $A_0 = 0$,$\tan\beta = 30$, $\mu > 0$ and $m_t = 175$ GeV (where $m_{\tilde{g}} = 1076$ GeV), versus various SM backgrounds.

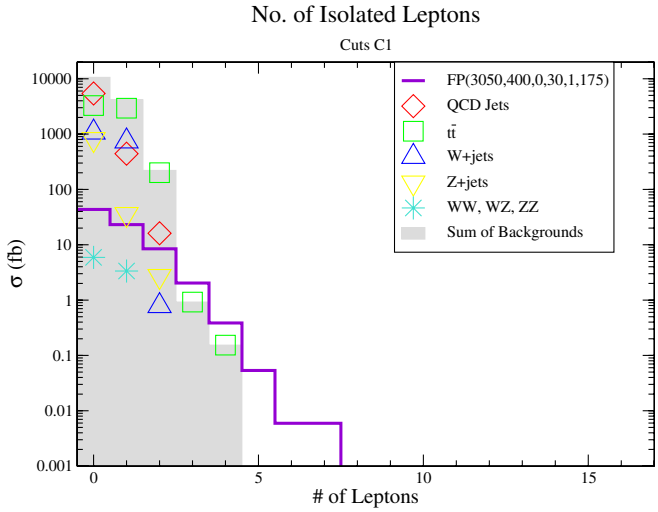

FIG. 8 (color online). Distribution of number of isolated leptons for the FP5 case study with $m_0 = 3050$ GeV, $m_{1/2} = 400$ GeV, $A_0 = 0$,$\tan\beta = 30$, $\mu > 0$ and $m_t = 175$ GeV (where $m_{\tilde{g}} = 1076$ GeV), versus various SM backgrounds.

At low $n(\text{jets}) \sim 4$–6, the distribution is dominated by QCD, $t\bar{t}$ and W, Z + jets production. However, at much higher jet multiplicities ~9–10, the signal distribution emerges[7] from the BG. Of course, at these high jet multiplicities, one may question the validity of the theoretical BG calculations. However, by investigating QCD multijet production and W, Z + jets production without imposing C1, it may be possible to normalize the expected BG distributions to measured data, and thus obtain after LHC turn-on improved estimates of expected BGs in these channels.

In Fig. 7, we show the expected multiplicity of b-jets for signal and SM BG. The soft component of signal is expected to be b-jet poor, since it comes from hadronic chargino and neutralino decays. However, the hard component is expected to typically contain at least 4 b-jets, aside from efficiency corrections. Indeed, we see that the signal distribution extends out to high b-jet multiplicities of $n(b - \text{jet}) \sim 5$–8, while the BG typically gives 0–2 b-jets. As noted previously, Mercadante *et al.* exploited this fact to enhance the LHC reach for SUSY in the HB/FP region [29].

In Fig. 8, we show the multiplicity of isolated leptons: electrons or muons. Again, while low lepton multiplicity is dominated by SM backgrounds, the high lepton multiplicity should be dominated by signal, owing to the lengthy gluino cascade decays, which can spin off additional isolated leptons at various stages.

At this point, it is evident that requiring collider events with high jet and high b-jet multiplicity will aid in separating signal from BG in the HB/FP region. Thus, in Fig. 9, we show the *augmented* effective mass distribution A_T, where

$$A_T = E_T^{\text{miss}} + \sum_{\text{leptons}} E_T + \sum_{\text{jets}} E_T, \tag{8}$$

which gives the added contribution of additional jets beyond $n(\text{jets}) = 4$ and also a contribution from isolated leptons. The distributions in Fig. 9 all contain, along with cuts C1, $n(\text{jets}) \geq 6$ and a) $n(b - \text{jets}) \geq 0$, b) $n(b - \text{jets}) \geq 1$, c) $n(b - \text{jets}) \geq 2$ and d) $n(b - \text{jets}) \geq 3$. As we move to higher b-jet multiplicity, the signal distribution begins to stand out clearly from BG, which is dominated at this point by $t\bar{t}$ production.

Alternatively, we can move to higher jet multiplicity. In Fig. 10, we again plot A_T but this time for $n(\text{jets}) \geq 7$ and $n(b - \text{jets}) \geq 2$. The signal emerges from the BG clearly above $A_T \sim 1300$–1400 GeV, and has an advantage over Fig. 9(d) in that a somewhat larger signal rate remains after cuts. For the case shown, by imposing $A_T > 1400$ GeV, we are left with a signal cross section for case FP5 of 11.1 fb, while BG from $t\bar{t}$ production is at the 1.5 fb level with a tiny contribution from QCD multijet production. In addition, the remaining signal is 98% from gluino pair production, so is almost entirely from the hard component of the signal.

V. SIGNAL, BACKGROUND AND SPARTICLE MASS EXTRACTION

We will adopt the cuts of Sec. IV as our cut set C2:

C2 Cuts:

$$\text{apply cut set C1} \qquad n(\text{jets}) \geq 7$$
$$n(b - \text{jets}) \geq 2 \qquad A_T \geq 1400 \text{ GeV}.$$

[7]The use of the steps in the jet multiplicity was introduced in Ref. [42] in extracting the signal of top quark pair production.

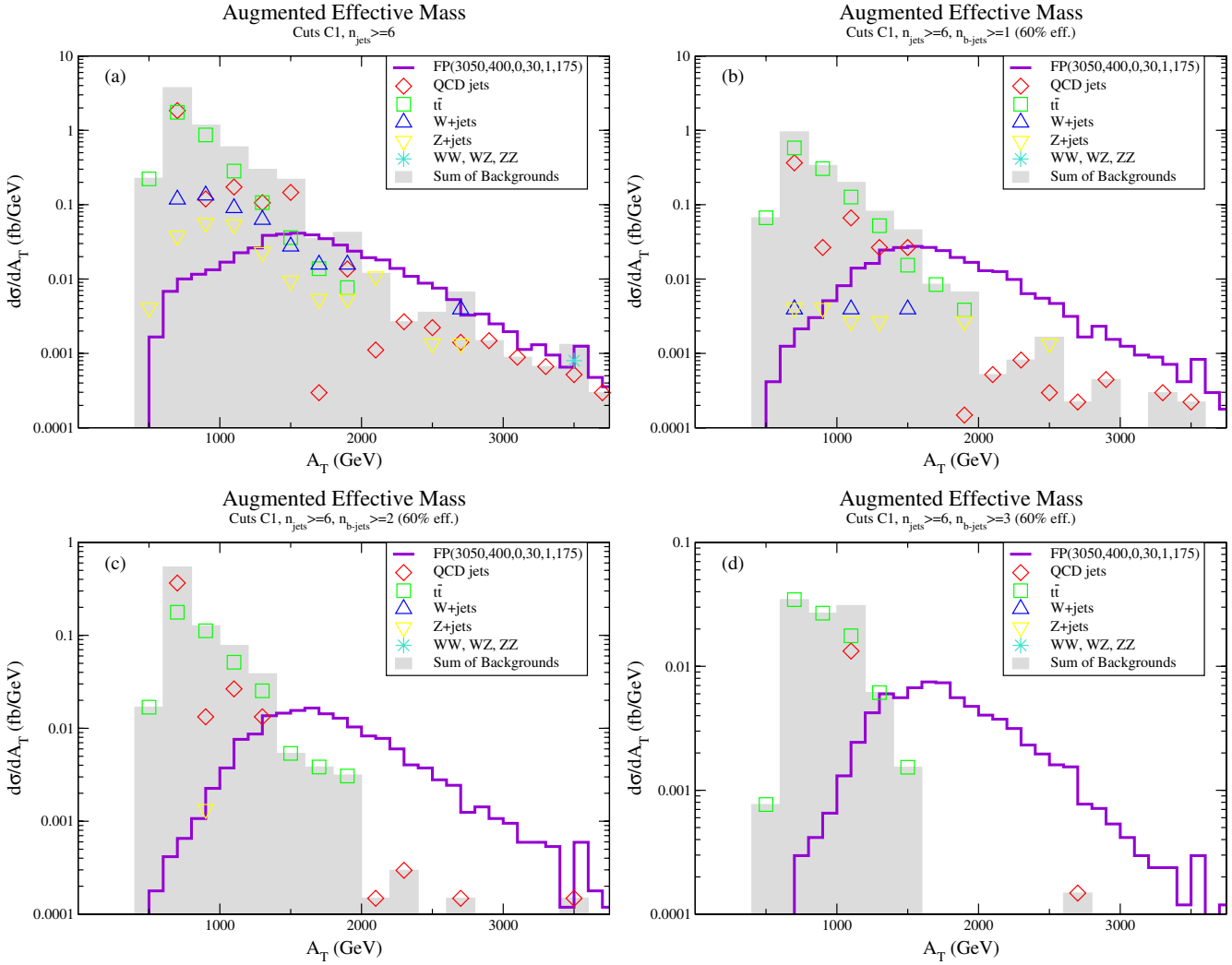

FIG. 9 (color online). Distribution in A_T [defined in Eq. (8)] in events with $n(\text{jets}) \geq 6$ with varying number of b-tags, for the FP5 case study with $m_0 = 3050$ GeV, $m_{1/2} = 400$ GeV, $A_0 = 0$,$\tan\beta = 30$, $\mu > 0$ and $m_t = 175$ GeV (where $m_{\tilde{g}} = 1076$ GeV), versus various SM backgrounds.

These cuts have been optimized for $m_{\tilde{g}} \sim 1$ TeV. Next, we plot in Fig. 11 the event rate after C2 versus $m_{\tilde{g}}$ along a line of FP region with $\Omega_{\tilde{Z}_1} h^2 \sim 0.11$, with $\tan\beta = 30$, $A_0 = 0$ and $\mu > 0$. For $m_{\tilde{g}} \lesssim 700$ GeV, $m_{\tilde{W}_1} < 103.5$ GeV, so the region is excluded by LEP2 chargino pair searches. The solid blue curve denotes the signal rate after cuts C2, while the brown dot-dashed curve denotes SM BG. Signal rates are typically in the multi-fb regime, and exceed BG out to $m_{\tilde{g}} \sim 1500$ GeV.

Since the signal in Fig. 11 comes from nearly pure $\tilde{g}\,\tilde{g}$ production, the total rate can be used as an absolute measure of the gluino mass. There are of course a variety of theoretical uncertainties which arise. One comes from how well-known is the absolute gluino pair production cross section. The value of $\sigma(\tilde{g}\,\tilde{g})$ has been computed to NLO in QCD in Ref. [37], where it is shown that a variation in renormalization/factorization scale leads to an uncertainty in $\sigma(\tilde{g}\,\tilde{g})$ of $\pm 11\%$. A further uncertainty arises from variations in the squark mass. Here, we are assuming decoupled scalars, so variation due to changes in $m_{\tilde{q}}$ are expected to be small. Nonetheless, we find that by varying $m_{\tilde{q}}$: 2–5 TeV, the cross section still varies by $\pm 10\%$. Folding the NLO uncertainty in quadrature with the $m_{\tilde{q}}$ uncertainty, we estimate the cross section uncertainty at $\pm 15\%$, and plot the expected theory cross section variation as the blue dashed lines.

At this point, it can be asked how well will we know the gluino branching fractions, upon which the signal rate also depends. Here, we remark that in the region with decoupled scalars, we are relying on a value of μ that is just right so that the neutralino LSP saturates the CDM relic density measurement. Small variations in μ about this region are found to lead to only small changes in the gluino branching fractions. This is shown in Fig. 12, where we plot in frame (a) variations in $\Omega_{\tilde{Z}_1} h^2$ versus μ, and in frame (b) variations in the dominant gluino branching fractions.

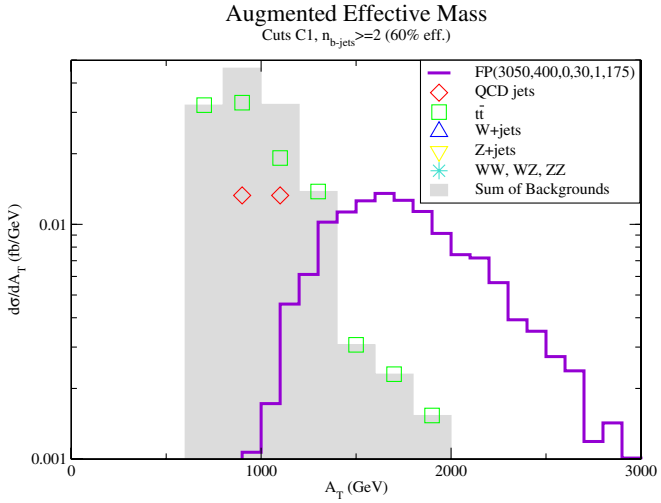

FIG. 10 (color online). Distribution of A_T in events with ≥ 7 jets and ≥ 2 b-tags, from the FP5 case study with $m_0 = 3050$ GeV, $m_{1/2} = 400$ GeV, $A_0 = 0$,tan$\beta = 30$, $\mu > 0$ and $m_t = 175$ GeV (where $m_{\tilde{g}} = 1076$ GeV), versus various SM backgrounds.

In the plot, we adopt as usual the case study FP5, and vary μ by adopting the nonuniversal Higgs soft mass model [43] in Isajet, which allows use of mSUGRA parameters, but also independent variation in the μ and m_A parameters (we keep m_A fixed).

It might also be argued that the event rate depends on the value of tanβ that we have selected for our case study. In fact, since scalar masses have decoupled, b and τ Yukawa coupling effects are tiny, and the variation of the signal

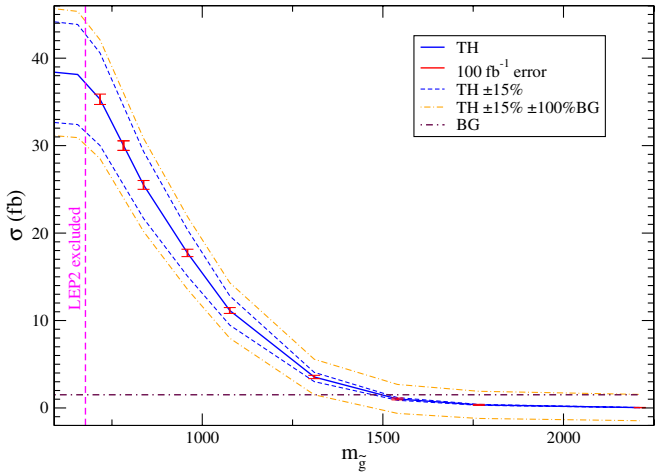

FIG. 11 (color online). Cross section after C1 plus ≥ 7 jets, ≥ 2 b-tags and $A_T > 1400$ GeV, for various points along the HB/FP region with $\Omega_{\tilde{Z}_1} h^2 \sim 0.11$ with $A_0 = 0$,tan$\beta = 30$, $\mu > 0$ and $m_t = 175$ GeV, versus $m_{\tilde{g}}$. We also show a band of the theoretically expected uncertainty of our results due to variations in factorization/renormalization scale and variations in $m_{\tilde{q}} \sim$ 2–5 TeV. We also show the level of expected SM background.

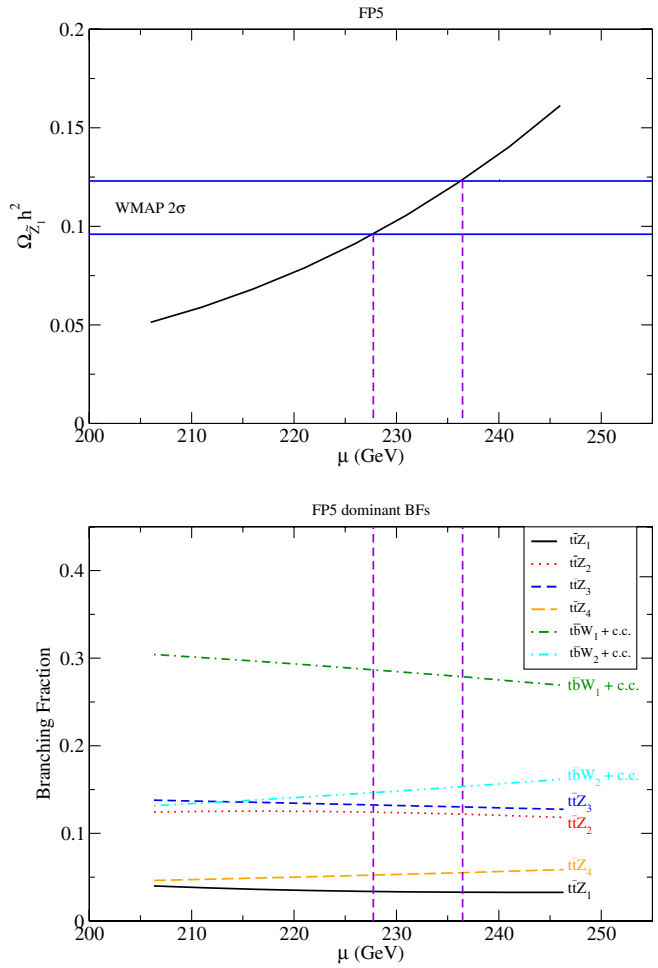

FIG. 12 (color online). (a) Variation in neutralino relic density with variation in μ for case study FP5. In (b), we show variation in dominat gluino branching fractions versus μ.

after cuts C2 with tanβ is comparatively negligible, as long as we require that the μ value be fixed so that one obtains the relic density $\Omega_{\tilde{Z}_1} h^2 \sim 0.11$. This is illustrated in Table IV, where we plot signal rate after cuts C2 for tan$\beta =$ 10, 20, 30, 40 and 50. In each case, the value of $m_{1/2}$ is fixed at 400 GeV, but m_0 is chosen so that the correct relic density is obtained. The resulting cross section after cuts C2 shows only a $\pm 6\%$ variability. Meanwhile, variations in

TABLE IV. Cross section after cuts C2 for HB/FP cases with $m_{1/2} = 400$ GeV, $A_0 = 0$, $\mu > 0$ and $m_t = 175$ GeV. We list the m_0 value required to give $\Omega_{\tilde{Z}_1} h^2 \sim 0.11$ for different tanβ values.

m_0	tanβ	σ(C2) (fb)
4090	10	9.92
3150	20	10.45
3050	30	11.15
3000	40	11.04
2970	50	11.17

the A_0 parameter again mainly affect the scalar sector, but since these decouple, the effects should again be small.

A further consideration is to ask how well we really know our background estimates. At this stage, the answer is difficult to know, and depends on several factors, including how well the selected event generator, Isajet, models SM backgrounds. If indeed $t\bar{t}$ production is the dominant BG, then the plethora of $t\bar{t}$ events produced at the LHC will allow detailed study of this reaction, so that the distributions will be well-known from data. Better theory modeling—such as inclusion of exact matrix elements for extra jet radiation [44]—will also help. Likewise, it can be expected that W + jets, Z + jets and QCD backgrounds will also be well studied, and the high n(jet) and high A_T tails will be better known due to actual collider measurements. In any case, we try to make a rough estimate by simply assuming that our event generator background is known to $\pm 100\%$. We add and subtract this BG uncertainty to our theory curves in Fig. 11, with the resultant band being denoted by orange dashed lines.

At this point, we can try to estimate the precision with which the gluino mass can be extracted from total cross section measurements. We show in Fig. 11 as data points the error bars expected from measuring the total cross section after cuts C2 with an assumed 100 fb^{-1} of integrated luminosity (red data points). A simple estimate of the uncertainty can be gained from the intersection of the upper and lower limits on the statistical cross section measurement with the band of theory uncertainty. Using this method, we find that points 2–6 yield a gluino mass measured in the range of $\pm 8\%$, as shown in Table I. The precision will increase or decrease depending on the ultimate uncertainty ascribed to the BG by the experimental groups. It would also decrease if an NNLO computation of gluino pair production is made. Note that even if the statistical error bars drop to zero (infinite integrated luminosity), the theory uncertainty still gives $\sim 7\%$ uncertainty. FP1—which is below the LEP2 excluded boundary—is difficult to measure because the projected theory curves level off for lower values of $m_{\tilde{g}}$. This is just a result of the fact that we optimized cuts in the 1 TeV $m_{\tilde{g}}$ region. A better optimization with softer cuts would need to be performed to extract these lower gluino masses. For $m_{\tilde{g}} \gtrsim 1300$ GeV, another optimization would be needed with harder cuts. Here, the absolute gluino pair event rate is dropping, so we expect a rate-based measurement of $m_{\tilde{g}}$ would be more challenging and perhaps not feasible in this higher mass region.

VI. LEPTONIC SIGNATURES

While the analysis in Sec. V focussed on lepton-inclusive signals, it is also useful to make use of the isolated lepton content of the signal. We expect events containing multiple isolated leptons to have somewhat reduced jet multiplicity compared to events with zero or one isolated lepton. To proceed with the multilepton channels, we retained cuts C1 and examined the A_T distribution maintaining $n(b-\text{jets}) \geq 2$ but requiring $n(\text{jets}) \geq 4$ or 5. The distribution in A_T for $n(\text{jets}) \geq 4$ is shown in Fig. 13. Here we see signal emerging from BG for $A_T > 1200$ GeV. (The plot using $n(\text{jets}) \geq 5$ is similar, but with lower signal and BG rates.) Hence, we adopt cut set C3 for events with 2 or more isolated leptons:

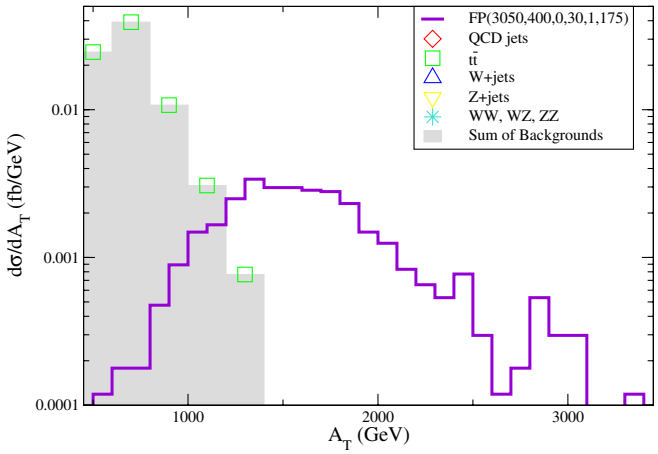

FIG. 13 (color online). Distribution in A_T of events with cuts C1, $n(\text{leps}) \geq 2$, $n(b-\text{jets}) \geq 2$ and $n(\text{jets}) \geq 4$ for the FP5 case study with $m_{\tilde{g}} = 1076$ GeV.

C3 Cuts:

$$\text{cuts set C1} \qquad n(\text{isol.leptons}) \geq 2 \qquad n(\text{jets}) \geq 4$$
$$n(b-\text{jets}) \geq 2 \qquad A_T \geq 1200 \text{ GeV}$$

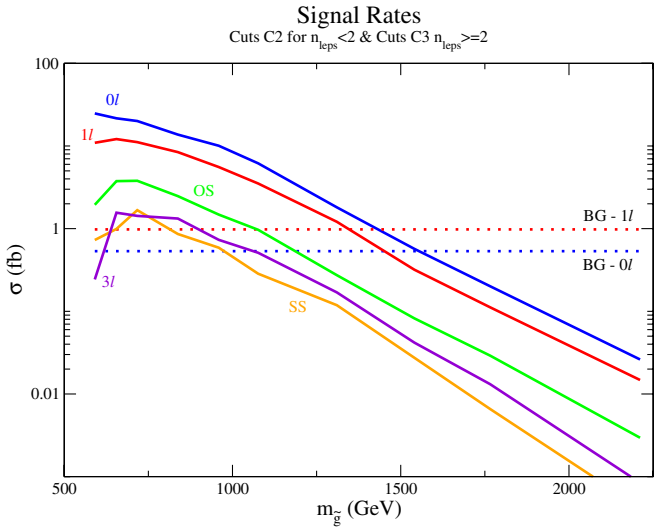

FIG. 14 (color online). Event rates for zero and one isolated lepton events after cuts C2, and OS and SS dileptons and trileptons after cuts C3, versus $m_{\tilde{g}}$. Zero and one lepton backgrounds are shown with the same color as the signal. We found no backgrounds events to OS, SS and 3l to the cross section level shown.

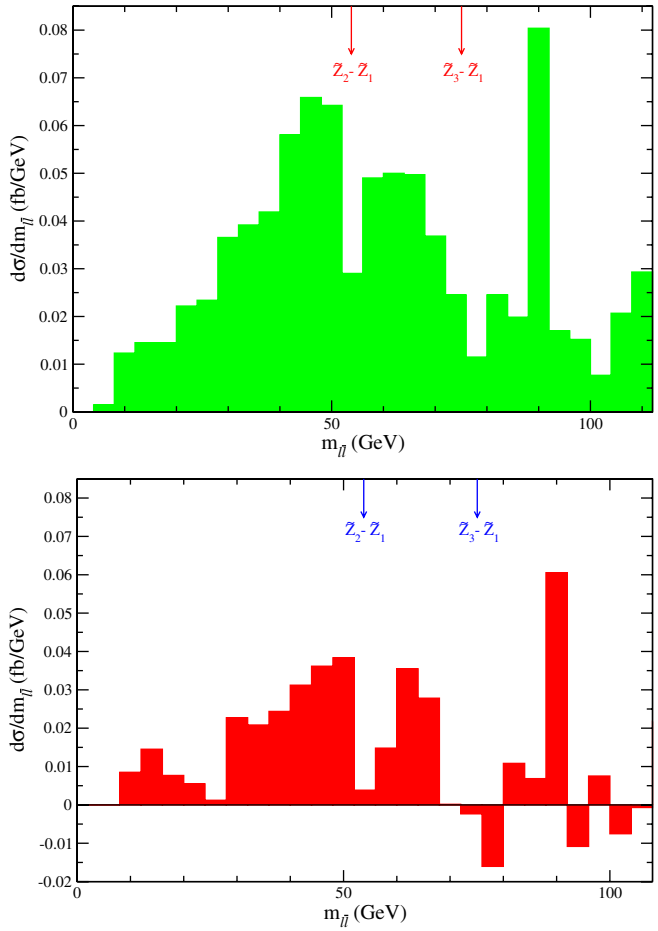

FIG. 15 (color online). (a) Distribution in OS/SF dilepton invariant mass for case FP4 using cuts C3. Two mass edges are becoming apparent at a luminosity of 100 fb^{-1}, in addition to the Z peak. (b) Distribution in e^+e^- plus $\mu^+\mu^-$ minus $e^+\mu^-$ minus μ^+e^- invariant mass.

In Fig. 14, we show the signal rate of various multilepton topologies versus $m_{\tilde{g}}$ for FP cases with $A_0 = 0$, $\tan\beta = 30$ and $\mu > 0$. The zero and one lepton topologies use cuts C2, while the same-sign (SS) dilepton, opposite sign dilepton (OS) and trilepton rates use cuts C3. We see that there should be consistent signals above SM backgrounds in all the various multilepton channels for much of the mass range of $m_{\tilde{g}}$. Same sign lepton events would establish the Majorana nature of the gluino [45].

It is also well known that kinematic information on neutralino mass differences can be gleaned by examining the invariant mass distribution of opposite-sign/same-flavor dilepton pairs (OS/SF) [46]. We plot in Fig. 15(a) the invariant mass distribution for case study FP4. The HB/FP region is characterized by the fact that $m_{\tilde{Z}_2} - m_{\tilde{Z}_1} < M_Z$ *and* by $m_{\tilde{Z}_3} - m_{\tilde{Z}_1} < M_Z$, so that two-body spoiler decays of $\tilde{Z}_2$ and $\tilde{Z}_3$ are closed. We then expect two mass edges in the $m(\ell^+\ell^-)$ distribution: in the case of FP4, one is at $m_{\tilde{Z}_2} - m_{\tilde{Z}_1} = 53.8$ GeV and another at $m_{\tilde{Z}_3} - m_{\tilde{Z}_1} = 75.1$ GeV. Indeed, the double mass edge structure is becoming visible in the $M_{l\bar{l}}$ distribution with 100 fb^{-1} of data as shown in Fig. 15. The dominant background comes from $t\bar{t}$ production, which should give equal rates for OS/SF and OS/OF dileptons. This continuum background can be subtracted out on a statistical basis by plotting the OS/SF invariant mass distribution minus the OS/OF distribution as suggested by Hinchliffe and Paige [25]. This distribution is shown in frame (b), where the mass edges may be more transparent.

VII. CONCLUSIONS

In this paper, we have examined the sort of collider events to be expected at the CERN LHC for SUSY models in the HB/FP region of the mSUGRA model. We found that by requiring high jet and b-jet multiplicity, and a high effective mass cut, a rather pure signal emerged from a dominantly $t\bar{t}$ SM background. Since the signal came almost entirely from gluino pair production, and the decay branching fractions were fixed by assuming the neutralino relic density saturated the WMAP $\Omega_{\tilde{Z}_1}h^2$ measurement, the total signal rate could be used to extract an estimate of the gluino mass. Factoring in theory uncertainty on the total cross section and a $\pm 100\%$ error estimate on remaining background, we found that $m_{\tilde{g}}$ could be measured to a precision of about 8% for 100 fb^{-1} of integrated luminosity. This was our central result.

We note here that our conclusions apply more generally than to just the HB/FP region of the mSUGRA model. The key assumptions needed for our analysis are that:

(1) The flavor/CP conserving MSSM is the correct effective theory of nature at the weak scale, with the lightest neutralino as LSP.
(2) We assume gaugino mass unification, as occurs in many SUSY GUT and string models.
(3) We assume that scalars—the squarks and sleptons—decouple due to mass values beyond the few TeV level. This leaves just the various gluinos, charginos and neutralinos contributing to LHC collider events.
(4) The value of μ is fixed by the requirement that the relic abundance of $\tilde{Z}_1$ saturates the WMAP measured value. This, along with gaugino mass unification, fixes the sparticle branching fractions to their assumed values.

If these conditions are fulfilled, then the methods presented here should allow for a gluino mass extraction if $m_{\tilde{g}}$ is in the mass range of ~700–1300 GeV. We note here that our result depends on the sparticle branching fractions being fixed to values near our calculated results. These in turn depend on the above assumptions being fulfilled. Thus, our study should be applicable to other heavy scalar situations, not only the HB/FP region of mSUGRA. Recently, such models have received renewed attention in light of FCNC constraints, and some string theory motivated models have produced heavier scalar spectra [47]. Our considerations

also apply to the low scalar mass regime of split SUSY models [48], where the gluino decays promptly inside collider detectors.

In addition, we note that the signal can be separated as to its isolated lepton content. Typically, for each additional isolated lepton, there should be on average 1.5 less jets per event. The OS/SF dilepton mass distribution embedded in the hard signal component should exhibit mass edges at $m_{\tilde{Z}_2} - m_{\tilde{Z}_1}$ and also at $m_{\tilde{Z}_3} - m_{\tilde{Z}_1}$, which are distinctive of this scenario in which the LSP is a mixed bino-Higgsino particle. The same mass edges should appear in the clean trilepton channel originating mainly from chargino-neutralino production (the soft component), as shown in Ref. [30]. The mass-difference edges, along with the absolute gluino mass, may provide enough information to constrain the absolute chargino and neutralino masses (including the LSP mass), under the assumptions listed above.

ACKNOWLEDGMENTS

This work was supported in part by the U.S. Department of Energy under grant No. DE-FG02-95ER40896, by the Wisconsin Alumni Research Foundation. We thank T. Krupovnickas and X. Tata for discussions. The work of L. W. is supported by the National Science Foundation under Grant No. 0243680 and the Department of Energy under Grant No. DE-FG02-90ER40542. Any opinions, findings, and conclusions or recommendations expressed in this material are those of the author(s) and do not necessarily reflect the views of the National Science Foundation.

[1] E. Cremmer, S. Ferrara, L. Girardello, and A. van Proeyen, Nucl. Phys. **B212**, 413 (1983).

[2] A. Chamseddine, R. Arnowitt, and P. Nath, Phys. Rev. Lett. **49**, 970 (1982); R. Barbieri, S. Ferrara, and C. Savoy, Phys. Lett. **119B**, 343 (1982); N. Ohta, Prog. Theor. Phys. **70**, 542 (1983); L. J. Hall, J. Lykken, and S. Weinberg, Phys. Rev. D **27**, 2359 (1983); for reviews, see H. P. Nilles, Phys. Rep. **110**, 1 (1984); P. Nath, arXiv:hep-ph/0307123.

[3] For an overview, see e.g. H. Baer and X. Tata, *Weak Scale Supersymmetry* (Cambridge University Press, Cambridge, England, 2006).

[4] ISAJET v7.74, by H. Baer, F. Paige, S. Protopopescu, and X. Tata, arXiv:hep-ph/0312045.

[5] H. Baer, J. Ferrandis, S. Kraml, and W. Porod, Phys. Rev. D **73**, 015010 (2006).

[6] H. Baer, C. Balazs, and A. Belyaev, J. High Energy Phys. 03 (2002) 042.

[7] D. N. Spergel *et al.* (WMAP Collaboration), arXiv:astro-ph/0603449.

[8] H. Baer and M. Brhlik, Phys. Rev. D **53**, 597 (1996); V. Barger and C. Kao, Phys. Rev. D **57**, 3131 (1998).

[9] J. Ellis, K. Olive, Y. Santoso, and V. Spanos, Phys. Lett. B **565**, 176 (2003); H. Baer and C. Balazs, J. Cosmol. Astropart. Phys. 05 (2003) 006; U. Chattapadhyay, A. Corsetti, and P. Nath, Phys. Rev. D **68**, 035005 (2003); A. Lahanas and D. V. Nanopoulos, Phys. Lett. B **568**, 55 (2003); A. Djouadi, M. Drees, and J. Kneur, arXiv:hep-ph/0602001.

[10] J. Ellis, T. Falk, and K. Olive, Phys. Lett. B **444**, 367 (1998); J. Ellis, T. Falk, K. Olive, and M. Srednicki, Astropart. Phys. **13**, 181 (2000); M. E. Gómez, G. Lazarides, and C. Pallis, Phys. Rev. D **61**, 123512 (2000); Phys. Lett. B **487**, 313 (2000); A. Lahanas, D. V. Nanopoulos, and V. Spanos, Phys. Rev. D **62**, 023515 (2000); R. Arnowitt, B. Dutta, and Y. Santoso, Nucl. Phys. **B606**, 59 (2001); H. Baer, C. Balazs, and A. Belyaev, J. High Energy Phys. 03 (2002) 042.

[11] C. Böhm, A. Djouadi, and M. Drees, Phys. Rev. D **62**, 035012 (2000); J. R. Ellis, K. A. Olive, and Y. Santoso, Astropart. Phys. **18**, 395 (2003); J. Edsjö *et al.*, J. Cosmol. Astropart. Phys. 04 (2003) 001.

[12] M. Drees and M. Nojiri, Phys. Rev. D **47**, 376 (1993); H. Baer and M. Brhlik, Phys. Rev. D **53**, 597 (1996); **57**, 567 (1998); H. Baer, M. Brhlik, M. Diaz, J. Ferrandis, P. Mercadante, P. Quintana, and X. Tata, Phys. Rev. D **63**, 015007 (2000); J. Ellis, T. Falk, G. Ganis, K. Olive, and M. Srednicki, Phys. Lett. B **510**, 236 (2001); L. Roszkowski, R. Ruiz de Austri, and T. Nihei, J. High Energy Phys. 08 (2001) 024; A. Djouadi, M. Drees, and J. L. Kneur, J. High Energy Phys. 08 (2001) 055; A. Lahanas and V. Spanos, Eur. Phys. J. C **23**, 185 (2002).

[13] R. Arnowitt and P. Nath, Phys. Rev. Lett. **70**, 3696 (1993); H. Baer and M. Brhlik, Ref. [8]; A. Djouadi, M. Drees, and J. Kneur, Phys. Lett. B **624**, 60 (2005).

[14] K. L. Chan, U. Chattopadhyay, and P. Nath, Phys. Rev. D **58**, 096004 (1998).

[15] J. Feng, K. Matchev, and T. Moroi, Phys. Rev. Lett. **84**, 2322 (2000); Phys. Rev. D **61**, 075005 (2000); **63**, 095003 (2001); J. Feng and F. Wilczek, Phys. Lett. B **631**, 170 (2005).

[16] The HB/FP region appears much earlier in H. Baer, C. H. Chen, F. Paige, and X. Tata, Phys. Rev. D **52**, 2746 (1995); **53**, 6241 (1996), but is not named, and fine-tuning is not addressed.

[17] H. Baer, C. H. Chen, F. Paige, and X. Tata, Ref. [16]; H. Baer, C. H. Chen, M. Drees, F. Paige, and X. Tata, Phys. Rev. D **59**, 055014 (1999); S. Abdullin and F. Charles, Nucl. Phys. **B547**, 60 (1999); S. Abdullin *et al.* (CMS Collaboration), arXiv:hep-ph/9806366; B. Allanach, J. Hetherington, A. Parker, and B. Webber, J. High Energy Phys. 08 (2000) 017.

[18] H. Baer, C. Balazs, A. Belyaev, T. Krupovnickas, and X. Tata, J. High Energy Phys. 06 (2003) 054.

[19] H. Baer, A. Belyaev, T. Krupovnickas, and X. Tata, J. High

Energy Phys. 02 (**2004**) 007; H. Baer, T. Krupovnickas, and X. Tata, J. High Energy Phys. 06 (2004) 061.

[20] H. Baer and X. Tata, Phys. Rev. D **47**, 2739 (1993).

[21] V. D. Barger and C. Kao, Phys. Rev. D **60**, 115015 (1999); H. Baer, M. Drees, F. Paige, P. Quintana, and X. Tata, Phys. Rev. D **61**, 095007 (2000); K. Matchev and D. Pierce, Phys. Lett. B **467**, 225 (1999).

[22] H. Baer, T. Krupovnickas, and X. Tata, J. High Energy Phys. 07 (2003) 020.

[23] For a recent analysis, see H. Baer, C. Balazs, A. Belyaev, and J. O'Farrill, J. Cosmol. Astropart. Phys. 09 (2003) 007; a subset of earlier work includes M. Goodman and E. Witten, Phys. Rev. D **31**, 3059 (1985); K. Griest, Phys. Rev. Lett. **61**, 666 (1988); Phys. Rev. D **38**, 2357 (1988); **39**, 3802(E) (1989); M. Drees and M. Nojiri, Phys. Rev. D **47**, 4226 (1993); **48**, 3483 (1993); V. A. Bednyakov, H. V. Klapdor-Kleingrothaus, and S. Kovalenko, Phys. Rev. D **50**, 7128 (1994); P. Nath and R. Arnowitt, Phys. Rev. Lett. **74**, 4592 (1995); L. Bergstrom and P. Gondolo, Astropart. Phys. **5**, 263 (1996); H. Baer and M. Brhlik, Phys. Rev. D **57**, 567 (1998); J. Ellis, A. Ferstl, and K. Olive, Phys. Lett. B **481**, 304 (2000); Phys. Rev. D **63**, 065016 (2001); E. Accomando, R. Arnowitt, B. Dutta, and Y. Santoso, Nucl. Phys. **B585**, 124 (2000); A. Bottino, F. Donato, N. Fornengo, and S. Scopel, Phys. Rev. D **63**, 125003 (2001); M. E. Gomez and J. D. Vergados, Phys. Lett. B **512**, 252 (2001); A. B. Lahanas, D. V. Nanopoulos, and V. C. Spanos, Phys. Lett. B **518**, 94 (2001); A. Corsetti and P. Nath, Phys. Rev. D **64**, 125010 (2001); E. A. Baltz and P. Gondolo, Phys. Rev. Lett. **86**, 5004 (2001); M. Drees, Y. G. Kim, T. Kobayashi, and M. M. Nojiri, Phys. Rev. D **63**, 115009 (2001); see also J. Feng, K. Matchev, and F. Wilczek, Phys. Lett. B **482**, 388 (2000); Phys. Rev. D **63**, 045024 (2001); R. Ellis, A. Ferstl, K. A. Olive, and Y. Santoso, Phys. Rev. D **67**, 123502 (2003); J. R. Ellis, K. A. Olive, Y. Santoso, and V. C. Spanos, Phys. Rev. D **69**, 015005 (2004); see C. Muñoz, arXiv:hep-ph/0309346 for a recent review.

[24] J. Feng, K. Matchev, and F. Wilczek, Phys. Lett. B **482**, 388 (2000); Phys. Rev. D **63**, 045024 (2001); H. Baer, A. Belyaev, T. Krupovnickas, and J. O'Farrill, J. High Energy Phys. 08 (2004) 005.

[25] I. Hinchliffe and F. Paige, in Workshop on Physics at TeV Colliders, Les Houches, France, 2001.

[26] H. Baer, V. D. Barger, and R. J. N. Phillips, Phys. Rev. D **39**, 3310 (1989).

[27] R. Arnowitt, B. Dutta, T. Kamon, N. Kolev, and D. Toback, Phys. Lett. B **639**, 46 (2006); R. Arnowitt, A. Aurisano, B. Dutta, T. Kamon, N. Kolev, D. Toback, P. Simeon, and P. Wagner, arXiv:hep-ph/0608193.

[28] U. Chattapadhyay, A. Data, A. Datta, A. Datta, and D. P. Roy, Phys. Lett. B **493**, 127 (2000).

[29] P. G. Mercadante, J. K. Mizukoshi, and X. Tata, Phys. Rev. D **72**, 035009 (2005).

[30] H. Baer, T. Krupovnickas, S. Profumo, and P. Ullio, J. High Energy Phys. 10 (2005) 020.

[31] E. Baltz, M. Battaglia, M. Peskin, and T. Wizansky, Phys. Rev. D **74**, 103521 (2006).

[32] H. Baer, V. D. Barger, D. Karatas, and X. Tata, Phys. Rev. D **36**, 96 (1987).

[33] H. Bachacou, I. Hinchliffe, and F. E. Paige, Phys. Rev. D **62**, 015009 (2000); B. C. Allanach, C. G. Lester, M. A. Parker, and B. R. Webber, J. High Energy Phys. 09 (2000) 004; C. G. Lester, M. A. Parker, and M. J. White, J. High Energy Phys. 01 (2006) 080; B. K. Gjelsten, D. J. Miller, and P. Osland, J. High Energy Phys. 12 (2004) 003.06 (2005) 015.

[34] A. Alves, O. Eboli, and T. Plehn, Phys. Rev. D **74**, 095010 (2006).

[35] V. D. Barger, M. S. Berger, and P. Ohmann, Phys. Rev. D **47**, 1093 (1993); S. P. Martin and M. T. Vaughn, Phys. Rev. D **50**, 2282 (1994).

[36] E. Brubaker *et al.*, arXiv:hep-ex/0608032.

[37] W. Beenakker, R. Hopker, M. Spira, and P. Zerwas, Nucl. Phys. **B492**, 51 (1997).

[38] H. Baer, X. Tata, and J. Woodside, Phys. Rev. D **42**, 1568 (1990); **45**, 142 (1992).

[39] V. D. Barger, A. L. Stange, and R. J. N. Phillips, Phys. Rev. D **45**, 1484 (1992).

[40] I. Hinchliffe, F. Paige, M. Shapiro, J. Söderqvist, and W. Yao, Phys. Rev. D **55**, 5520 (1997).

[41] V. Barger and R. J. N. Phillips, *Collider Physics* (Addison-Wesley, Reading, MA, 1987).

[42] H. Baer, V. D. Barger, and R. J. N. Phillips, Phys. Lett. B **221**, 398 (1989).

[43] H. Baer, A. Mustafayev, S. Profumo, A. Belyaev, and X. Tata, J. High Energy Phys. 07 (2005) 065.

[44] H. Baer, C. H. Chen, and M. H. Reno, Phys. Rev. D **48**, 5168 (1993).

[45] V. D. Barger, W. Y. Keung, and R. J. N. Phillips, Phys. Rev. Lett. **55**, 166 (1985).R. M. Barnett, J. F. Gunion, and H. E. Haber, Phys. Lett. B **315**, 349 (1993).

[46] H. Baer, K. Hagiwara, and X. Tata, Phys. Rev. D **35**, 1598 (1987); H. Baer, D. Dzialo-Karatas, and X. Tata, Phys. Rev. D **42**, 2259 (1990); H. Baer, C. Kao, and X. Tata, Phys. Rev. D **48**, 5175 (1993); H. Baer, C. H. Chen, F. Paige, and X. Tata, Phys. Rev. D **50**, 4508 (1994).

[47] See e.g. I. Antoniadis, K. Benakli, A. Delgado, M. Quiros, and M. Tuckmantel, Nucl. Phys. **B744**, 156 (2006); B. S. Acharya, K. Bobkov, G. L. Kane, P. Kumar, and J. Shao, arXiv:hep-th/0701034.

[48] A. Arkani-Hamed and S. Dimopoulos, J. High Energy Phys. 06 (2005) 073.